

Phase transitions of NH_4Cl under low temperature or high pressure observed by sequential powder x-ray diffraction

Kazuki Komatsu,^{*a} Takanori Murakami,^a Satoshi Nakano^b and Hiroyuki Kagi^a

- a. Geochemical Research Centre, Graduate School of Science, The University of Tokyo, 7-3-1 Hongo, Bunkyo-ku, Tokyo 113-0033, Japan. E-mail: kom@eqchem.s.u-tokyo.ac.jp
- b. National Institute for Materials Science (NIMS), 1-1 Namiki, Tsukuba, Ibaraki 305-0044, Japan.

Abstract

The compression behavior and phase transitions of NH_4Cl were investigated using x-ray diffraction. A clear volume anomaly at 0.7–1.0 GPa confirmed the first-order nature of the phase II–IV transition at 298 K. Low-temperature x-ray diffraction measurements at ambient pressure revealed a slight hysteresis in this transition, suggesting differences in the degree of order of the orientation of NH_4^+ ion in the cooling and heating processes. We first clarified that the crystal structure of phase V has antiferro-ordered orientation with tetragonal system, and the structural analysis of phase V indicated that hydrogen bonding plays a key role in the alternately varied N-Cl distances.

Introduction

The orientational order-disorder phase transition of ammonium halides caused by the orientation of ammonium ions has long been a subject of interest. The characteristic heat capacity anomaly, first observed in NH_4Cl at 242-243 K by Simon in 1922¹, became the origin of the term " λ -transition" and subsequently served as a prototype for numerous studies on orientational order-disorder transitions². The behavior of ammonium halides under high pressure has also been extensively studied since the early work of Bridgman³. These studies demonstrated that the order-disorder phase transition observed at low temperatures and ambient pressure also occurs at high pressures and room temperature. Moreover, the transition pressure systematically varies depending on the type of anion. In recent years, the high-pressure behavior of ammonium halides has been revisited in various contexts, such as their giant barocaloric effect⁴, their potential as high-temperature superconductors⁵ or hydrogen storage materials⁶, and their relevance as structural analogs of ice⁷.

The orientational order of ammonium ions also contributes to the polymorphic diversity of ammonium halides. Here we aim to clarify the nomenclature of NH_4Cl polymorphs, since there has been some confusion. Under ambient conditions at room temperature, NH_4Cl adopts the CsCl-type cubic structure ($Pm\bar{3}m$), designated as phase II or β phase (Figure 1). In phase II, NH_4^+ ions exhibit static disorder. Above 458 K at ambient pressure, NH_4^+ ions become dynamically disordered with the NaCl-type cubic structure ($Fm\bar{3}m$), forming a so-called plastic state, referred to as phase I or α phase. Below 243 K at ambient pressure, NH_4^+ ions adopt a ferro-ordered state, initially called phase III or the δ -phase (e.g., ^{8, 9}). However, to maintain consistency with the nomenclature of isostructural polymorphs in NH_4I and NH_4Br , the ferro-ordered phase has been increasingly referred to as phase IV instead of phase III in literature since the 1990s (e.g., ^{5, 10}). In this study, we follow this convention and refer to this ferro-ordered phase as phase IV. Furthermore, it is known that phase II transitions to phase IV at approximately 1 GPa at room temperature⁸. At pressures above ~ 11 GPa, phase IV undergoes a transition to an antiferro-ordered phase V, as indicated by Raman spectroscopy^{11, 12}. The structure of phase V has been confirmed in NH_4I by angle-dispersive x-ray diffraction to be an antiferro-ordered phase¹³; however, no diffraction-based structural studies have been reported for NH_4Cl to date. Notably, despite the apparent isostructurality of phases III and V, as both exhibit antiferro-ordered NH_4^+ ions, they have historically been assigned different names. In this study, we adhere to the conventional nomenclature[†] and refer to the high-pressure phase of phase IV as phase V.

The phase transitions in ammonium halides are also of theoretical interest, particularly regarding the order of the transition between phase II and IV. For instance, Weiner and Garland¹⁴ suggested the existence of a second-order phase transition at 0.28 GPa and 267 K, whereas others have reported that the transition remains first-order across all pressure ranges (e.g., ⁸). Some later studies (e.g., ¹⁵) cited evidence for a tricritical phase transition at 0.16 GPa and 257 K; however, experimental verification remains insufficient.

In this study, we conducted in-situ x-ray diffraction experiments on NH_4Cl , varying temperature from 10 K to 300 K at ambient pressure and applying pressures up to 15.1 GPa at 298 K. Our investigation focused

on the structural changes associated with the II-IV and IV-V transitions to elucidate their phase transition mechanisms.

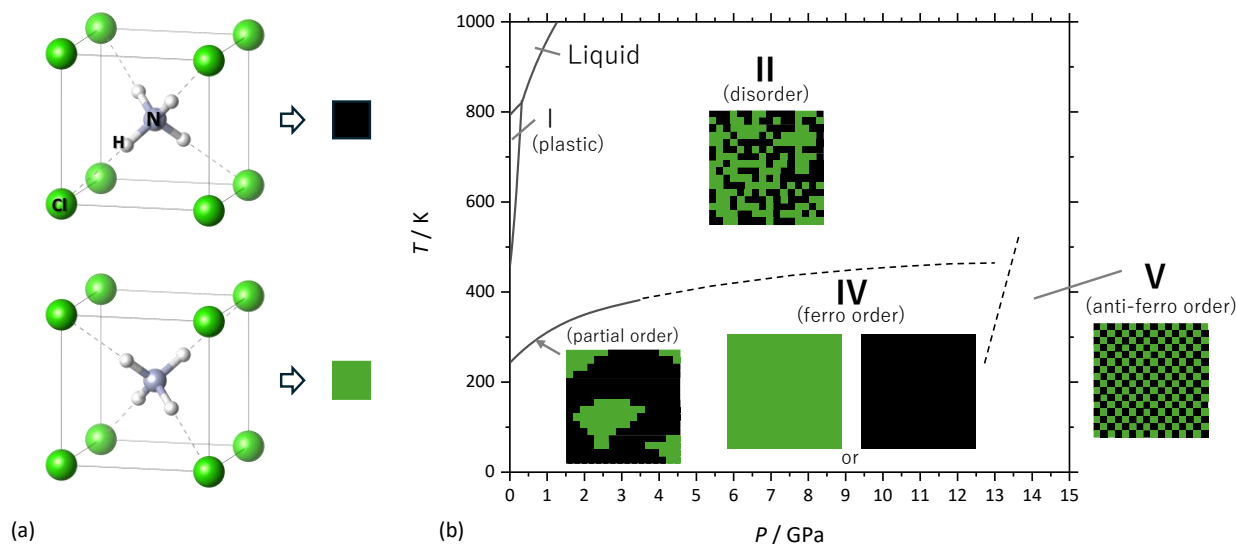


Fig. 1 (a) Two possible orientations of NH_4^+ ion in NH_4Cl crystal structure. One orientation is schematically depicted as a black square, while the other orientation is green. (b) Phase diagram of NH_4Cl with schematic images showing respective structures in terms of the orientation of NH_4^+ ion as depicted in (a). The phase boundary below 4 GPa is from ref.⁸ The broken lines show extrapolated from the previous study⁸ or estimated phase boundaries from previous Raman spectroscopic studies^{11, 12} and from x-ray diffraction in this study (see text in details).

Experimental methods

Sample preparation

Reagent-grade NH_4Cl (>99.5% purity, Wako) was used in this study. To prepare a fine powder sample for x-ray diffraction, it was ground inside a nitrogen-filled glovebox to prevent moisture absorption. Additionally, grinding was performed on a heated hotplate to remove any residual water.

Powder x-ray diffraction at high pressures

For high-pressure experiments, NaCl, a pressure marker to determine the applied pressure from the diffraction pattern, was ground together with NH_4Cl (weight ratio 4:1). The NH_4Cl and NaCl mixture was loaded in diamond anvil cells (DACs) with Daphne 7575 oil as a pressure-transmitting

medium (PTM)¹⁶. A pair of diamonds with a culet size of 600 μm and with Boeler-Almax type conical seats were used as anvils. A SUS301 stainless steel gasket with a hole diameter of 300 μm was used.

The powder x-ray diffraction experiment was conducted at BL-18C in Photon Factory (PF), High Energy Accelerator Research Organization (KEK), Japan. The x-ray beam ($\lambda = 0.6192 \text{ \AA}$) was irradiated to the sample through the collimator with a diameter of 100 μm . The diffraction patterns were recorded using a flat panel detector (Rad-icon 2022 CMOS detector, Teledyne Rad-icon Imaging Corporation) with an exposure time of 1 min. The obtained 2D patterns were converted to 1D patterns by using IPAnalyzer & PDIndexer softwares¹⁷. The wavelength of the incident x-ray, the detector-sample distance, the orientation of the detector and the pixel size were calibrated using the reference sample CeO_2 .

In the powder x-ray diffraction experiments, bellows were attached to the DAC to control the load of the DAC by helium gas pressure, which was increased from 0.5 MPa to 2.5 MPa at the rate of 0.01 MPa/min. The helium gas pressure was controlled by a pressure controller, Druck PACE5000 (GE). 200 diffraction patterns were recorded while pressurizing the DAC by the bellows, each pattern corresponds to a load step of 0.01 MPa. Sample pressures were estimated from the unit cell parameters of NaCl ¹⁸, which were obtained by the LeBail analyses using EXPGUI/GSAS software¹⁹.

Powder x-ray diffraction under low temperature

For low-temperature powder x-ray diffraction, the samples were loaded into DACs made of a copper-beryllium alloy serving as sample holders without applying pressure. The temperature was controlled using a 4K GM cryostat (MiniStat, Iwatani Co.) equipped with a temperature control system (Model 335, Lakeshore). The temperature inside the cryostat was monitored by a pre-calibrated silicon diode thermometer connected to the base frame of the DAC, while the temperature difference between the silicon diode thermometer and the base frame of the DAC was precisely monitored by the T-type thermocouple attached to the diamond plate of the DAC. Every x-ray diffraction measurement was conducted after the temperature got steady, which was approximately 15 min after changing set-points of temperature.

Powder x-ray diffraction for structural analysis of phase V

The reagent powder of ammonium chloride was finely ground on an alumina mortar in a glovebox, and loaded into DACs with a small sphere of ruby. SUS301 stainless steel with a hole diameter of 0.2 mm was used as a gasket. High-pressure helium gas (180 MPa) was loaded into the sample chamber as a PTM to maintain hydrostatic conditions²⁰. Further load was applied to the DAC using a torque wrench, manually applying force by three screws.

The x-ray diffraction experiment was conducted at BL-18C, PF, KEK. The incident x-ray wavelength was 0.6195 \AA . When the x-ray diffraction pattern at 15.4 GPa was obtained, the DAC was rotated from 13 to 17 degrees to the incident X-ray beam. The diffraction patterns obtained at different

angles were averaged to reduce the effect of the preferred orientation and coarse crystals, and also to observe higher 2θ . The obtained diffraction pattern was analyzed by the Rietveld method using z-Rietveld software²¹. The initial atomic coordinates of phase V of NH_4Cl were derived from phase V of NH_4I ¹³. The unit cell parameters, atomic positions and atomic displacement parameters except for hydrogen, background coefficients, a scale factor, and profile function parameters were refined in the Rietveld analysis.

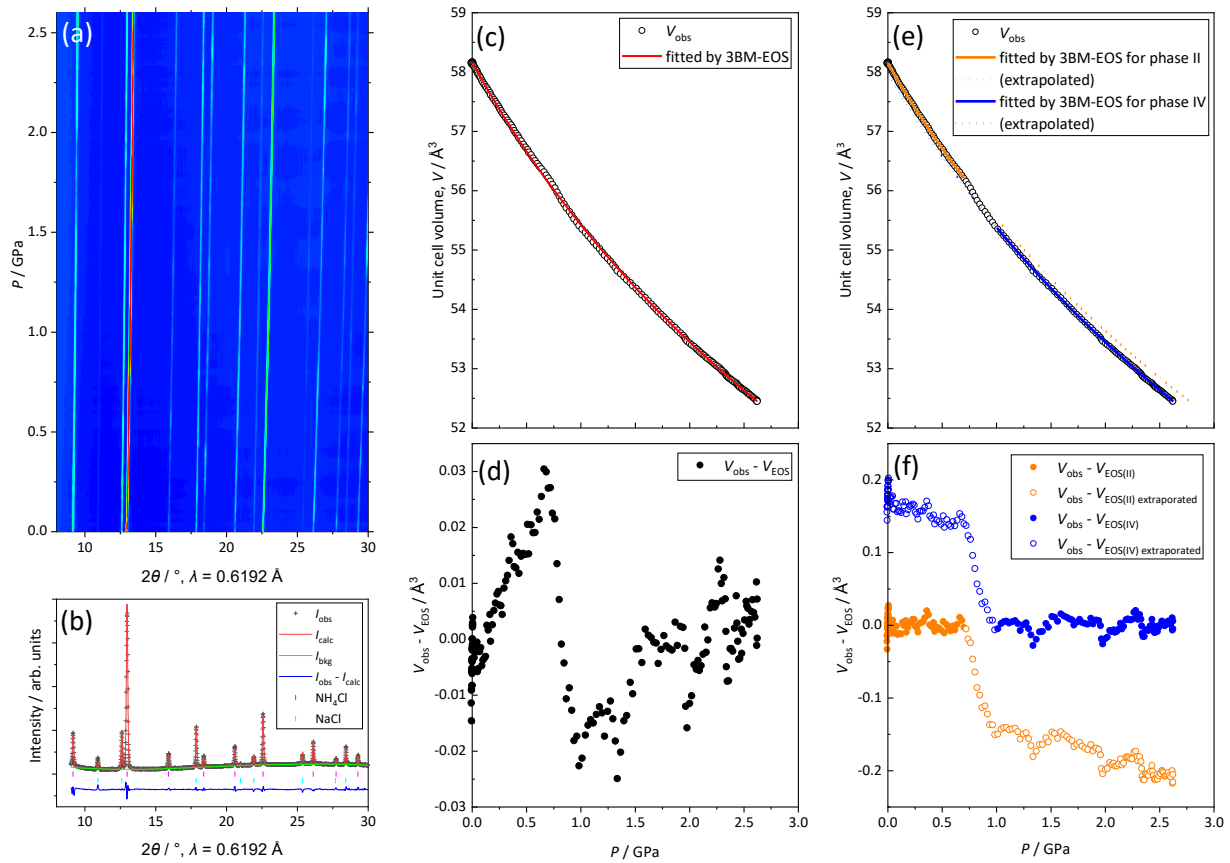


Fig. 2 (a) Color map of powder x-ray diffraction patterns of NH_4Cl with NaCl (pressure marker) with increasing pressure at 298 K. The color scale represents diffraction intensity, with blue indicating low intensity and red indicating high intensity. (b) A representative result of Le-Bail analysis for the diffraction pattern obtained at 0 GPa. (c) Observed unit-cell volume obtained by the Le-Bail analyses with the fitting curve by a 3rd-order Birch-Murnaghan equation of state (3BM-EOS) for the whole observed pressure region. (d) Difference between the observed unit-cell volume (V_{obs}) and the corresponding volume estimated from the 3BM-EOS (V_{EOS}). (e) Observed unit-cell volume fitted with the 3BM-EOS for the pressure regions from 0 to 0.7 GPa (phase II, orange), and from 1.0 to 2.6 GPa (phase IV, blue). The fitting curves are extrapolated, as shown in dotted lines. (f) Differences between V_{obs} and V_{EOS} estimated from the 3BM-EOS for phase II (orange) and phase IV (blue). Open circles depict the volume difference for the extrapolated pressure region.

Results and discussion

II-IV phase transition by isothermal compression

To investigate the pressure-dependent change in the unit cell volume of NH_4Cl at room temperature, we collected a total of 200 powder diffraction patterns from 0 GPa to 2.6 GPa (Fig. 2a). The Le Bail fitting was performed on these diffraction patterns to determine the unit cell volumes of NH_4Cl and NaCl , the latter serving as a pressure marker (Fig. 2b).

At first glance, the pressure evolution of NH_4Cl 's unit cell volume appears continuous (Fig. 2c). However, the deviation from the volume estimated by the third-order Birch-Murnaghan Equation of State (hereafter abbreviated as 3BM-EOS), as described in the following equation,

$$P = \frac{3K_0}{2} \left\{ \left(\frac{V_0}{V} \right)^{\frac{7}{3}} - \left(\frac{V_0}{V} \right)^{\frac{5}{3}} \right\} \left[1 + \frac{3}{4} (K'_0 - 4) \left\{ \left(\frac{V_0}{V} \right)^{\frac{2}{3}} - 1 \right\} \right] \quad (1)$$

clearly indicating a local maximum at 0.7 GPa and a local minimum at 1.0 GPa as shown in Fig. 2d.

This result indicates that the phase transition from phase II to phase IV begins at 0.7 GPa and completes at 1.0 GPa through a coexistence region, beyond which phase IV is fully occupied. The clear observation of a local maximum and minimum strongly suggests that this phase transition is first order. If the transition were second-order or higher, a coexistence region would not be expected, and the transition from phase II to phase IV would occur instantaneously at a single pressure point.

It is important to note that our experiments used Daphne 7575 as the PTM, which maintains hydrostaticity up to approximately 4.8 GPa. Since the pressure range of interest (0.7–1.0 GPa) is well below the solidification pressure of the medium, the pressure distribution in the sample chamber can be considered highly homogeneous. This ensures that the observed anomalies at 0.7 GPa and 1.0 GPa are not artefacts caused by pressure gradients. These findings contradict the previously reported claim that a tricritical point, marking the transition from a first-order to a second-order phase transition, exists at 0.16 GPa and 257 K.

Assuming that only phase II exists below 0.7 GPa and only phase IV exists above 1.0 GPa, we performed separate 3BM-EOS fittings for each phase (Fig. 2e). The deviations of the observed volumes from the fitted parameters were plotted in Fig. 2f. The bulk modulus (K_0), its pressure derivative (K'_0), and the unit cell volume at 0 GPa (V_0) were determined as follows:

- Phase II: $K_0 = 18.05(11)$ GPa, $K'_0 = 7.9(4)$, $V_0 = 58.152(2) \text{ \AA}^3$.

- Phase IV: $K_0 = 18.7(4)$ GPa, $K'_0 = 6.8(3)$, $V_0 = 57.97(4) \text{ \AA}^3$.

As shown in Fig. 2f, the volume change (ΔV) associated with the phase II to IV transition was determined to be 0.15 \AA^3 . To capture such a subtle volume change, it was necessary to collect a large number of data points with very small temperature or pressure increments. This requirement may have led to the phenomenon being overlooked in previous studies. In general, it is technically challenging to vary only the temperature under high-pressure conditions. This is because any change in temperature causes a corresponding change in the sample volume, which in turn alters

the pressure. In contrast, the present experiment was conducted under isothermal compression conditions, allowing us to independently vary the pressure while maintaining the temperature at room temperature. This capability was likely the key factor in successfully detecting the small volume change associated with the phase transition.

II-IV phase transition at ambient pressure

The results of x-ray diffraction patterns obtained at approximately 10 K intervals between 300 K and 10 K under ambient pressure are shown in Fig. 3a. During the cooling process from 300 K to 10 K, a clear discontinuity in the unit cell volume is observed between 240 K and 250 K (Fig. 3b). This volume change corresponds to the phase transition from phase II to phase IV at 243 K and is consistent with previous x-ray diffraction results²² (see also Figs 5 and 7 compiled in ref ²).

During the heating process from 10 K to 300 K, the unit cell volumes are almost identical to those observed during cooling, except in the range of 240 K to 230 K, where slightly smaller values are observed during the heating process. As shown in previous studies², this provides evidence of first-order phase transition associated with a slight hysteresis in the phase II–IV transition at ambient pressure, indicating a difference in the degree of ordering between the cooling and heating processes. In other words, during the cooling process, the disordered domains in the high-temperature phase partially persist, whereas during the heating process, the ordered orientation of the low-temperature phase remains.

To estimate the unit-cell volume of phase IV of NH₄Cl at ambient pressure, the observed data were fitted using the formula of thermal expansion shown below (Figure 3b).

$$V_{T,0} = V_{0,0} \exp \int_0^T \alpha_{T,0} dT$$

$$\alpha_{T,0} = m_0 + n_0 T, \quad (2)$$

where, $V_{T,0}$ is the unit-cell volume at T K and 0 GPa, $V_{0,0}$ is the unit-cell volume at 0 K and 0 GPa, and $\alpha_{T,0}$ is the thermal expansion coefficient at T K and 0 GPa. $V_{0,0}$, m_0 and n_0 are fitted parameters. The n_0 of phase II was fixed to 0, given that the temperature dependence of the thermal expansion coefficient $\alpha_{T,0}$ is constant within the narrow temperature range ($250 \text{ K} < T < 300 \text{ K}$). The results of the fitting are as follows:

- Phase II: $V_{0,0} = 55.21(6) \text{ \AA}^3$, $m_0 = 1.73(4) \times 10^{-4} \text{ K}^{-1}$.

- Phase IV: $V_{0,0} = 55.81(1) \text{ \AA}^3$, $m_0 = -1.7(4) \times 10^{-5} \text{ K}^{-1}$,

$$n_0 = 8.8(3) \times 10^{-7} \text{ K}^{-2}.$$

From the eq. (2) and fitted parameters, the unit-cell volume of phase IV extrapolated to 300 K is 57.8 \AA^3 , while the calculated unit-cell volume of phase II at 300 K using the eq. (2) is 58.2 \AA^3 . These values are well consistent with the unit-cell volume extrapolated from the 3BM-EOS ($58.152(2) \text{ \AA}^3$). The volume difference between phase II and IV at the phase transition temperature (243 K) is about 0.3 \AA^3 , which is nearly twice the volume difference observed at room temperature and high pressure.

The unit cell volumes below 70 K were observed for the first time in this study. Thermal expansion below 50 K was almost zero, or maybe slightly negative below 30 K, which is interesting in terms of the comparison to the similar phenomena found in ice²³, but here we would not go into the depth in this issue.

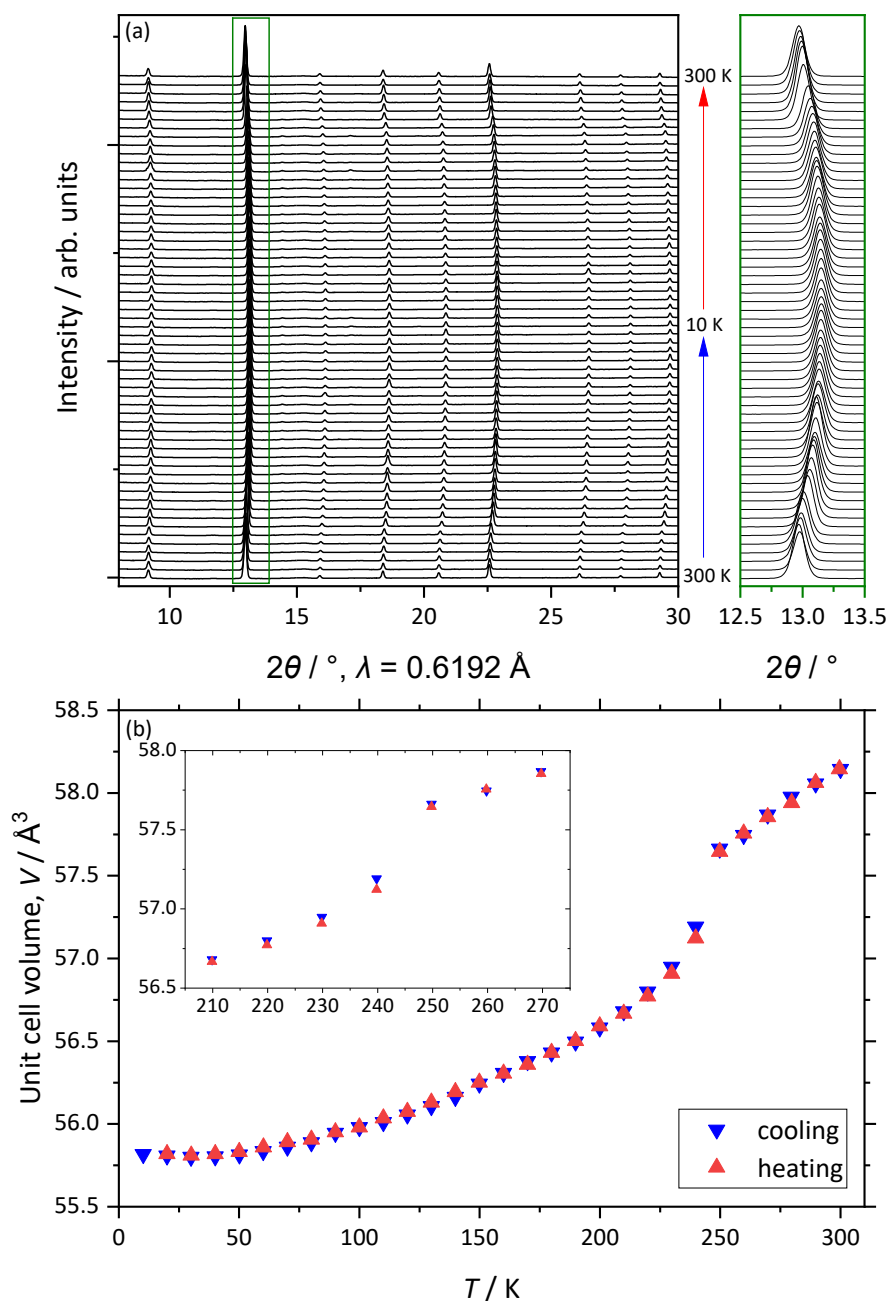


Fig. 3 (a) Sequential stacking plots of powder x-ray diffraction patterns of NH_4Cl , cooling from 300 K to 10 K and subsequent heating up to 300 K with approximately 10 K steps. The right-hand plots show enlarged diffraction patterns from 12.5° to 13.5° . (b) Temperature dependence of the unit-cell volume of NH_4Cl . The inset shows the enlarged plot around the phase II-IV transition.

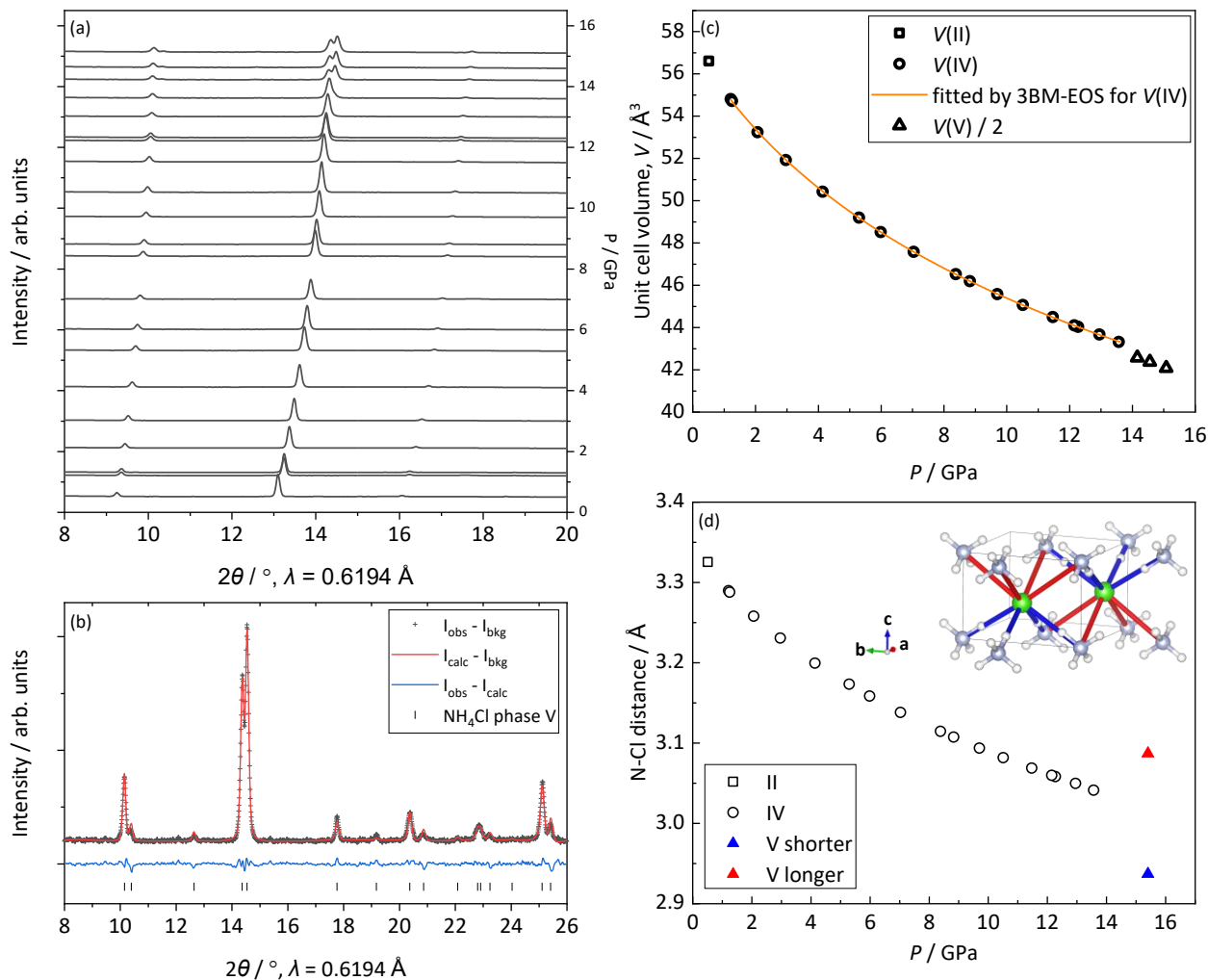


Fig. 4 (a) Sequential stacking plots of powder x-ray diffraction patterns of NH_4Cl with increasing pressure at 298 K. The diffraction patterns are shifted such that they intersect the right-hand vertical axis at their measurement pressure. (b) The result of Rietveld analysis for the diffraction pattern obtained at 15.1 GPa. The observed and calculated intensities are subtracted by the fitted background intensities for clarity. (c) Observed unit-cell volume of NH_4Cl phase II, IV and V (divided by two for comparison to phase II and IV), and the fitting curve by a 3BM-EOS for phase IV. (d) Distances between N and Cl at elevated pressure in phase II, IV and V. The N-Cl distances of phase II and IV are derived from unit-cell parameters, whereas that of phase V is determined by the Rietveld analysis. Only the data at 15.1 GPa are plotted for phase V, since other diffraction patterns have limited 2θ region up to 20° which is insufficient quality for the Rietveld analyses. The crystal structure depicted in the upper right of the plot represents phase V of NH_4Cl , where hydrogen-bonded N-Cl bonds are shown in blue, and non-hydrogen-bonded N-Cl bonds are shown in red. The solid-lined parallelepiped in the crystal structure represents the unit cell of phase V.

Crystal structure analysis of phase V and the unit-cell volume change of IV-V phase transition

For crystal structure determination of phase V, we used helium PTM since it is the only PTM which can be used above 10 GPa at 298 K⁵. The obtained powder x-ray diffraction patterns clearly indicate the peak splitting of 110 reflection of phase IV above 14 GPa (Fig 4a), associated with the volume reduction (Fig. 4c), which would be attributed to the phase transition from phase IV to V. The previous studies reported that the phase boundary between phase IV and V exists above 11 GPa¹¹ or 12.9 GPa¹², based on Raman spectroscopy. The phase transition pressure observed in this study is slightly higher than these previously reported values, which could be attributed to the difference in hydrostatic conditions or the difference of spectroscopy and diffraction methods.

Because this phase transition involves the tetragonal distortion with the volume change, it is clearly first-ordered phase transition. The Rietveld analysis for the diffraction pattern obtained at 15.1 GPa gives reasonably fitted well using the initial structural parameters from the phase V of NH₄I¹³. The results of the Rietveld analysis are summarized in Table 1. Note here that we could not determine hydrogen positions so that their parameters were fixed to the values reported in ¹³. Although it is highly likely that the crystal structure of phase V is identical to those of other ammonium halides, the hydrogen positions should be confirmed by neutron diffraction in future.

Table 1 Structural parameters of NH₄Cl phase V at 15.1 GPa and at 298 K from the Rietveld analysis.

Space group	<i>P4/nmm</i> (#129, origin choice 1)			
<i>Z</i>	2			
Unit cell parameters	<i>a</i> = 4.9587(3) Å			
	<i>c</i> = 3.4237(2) Å			
<i>R</i> factors	<i>R</i> _p = 0.9676%			
	<i>R</i> _{wp} = 1.3835%			
	<i>R</i> _F = 4.7207%			
	<i>S</i> = 3.2101			
Atomic positions and isotropic atomic displacement parameters				
Atom	<i>x</i>	<i>y</i>	<i>z</i>	<i>U</i> / Å ²
N	0	0	0	0.0051(8)
H	0	0.159*	0.159*	0.038**
Cl	0	0.5	0.4674(2)	0.0132(5)

*fixed to the reference value¹³.
**fixed to a typical value.

In NH_4Cl , each Cl^- ion is coordinated by eight NH_4^+ ions. In phases II and IV, the cubic symmetry ensures that all eight N-Cl distances are equivalent, and they can be calculated as $\sqrt{3}/2$ of the unit cell parameter, a (Fig. 4d). In contrast, in phase V, the symmetry lowers to tetragonal, resulting in a separation into four shorter and four longer N-Cl distances. Given that the hydrogen positions are correctly assigned, H atoms are located between the shorter N-Cl bonds but absent in the longer ones. This suggests that the presence or absence of N-H...Cl hydrogen bonds contributes to the variation in N-Cl distances. In phases II and IV, at least in the average structure derived from diffraction experiments, eight N-Cl distances are symmetrically equivalent. However, on a local scale, it is likely that N-Cl distances are shorter where hydrogen bonds are present. This kind of local structure could be observed from neutron total scattering as is conducted for phase II and IV of NH_4Br ²⁴. In phase V, the effect of N-H...Cl hydrogen bonding on N-Cl distances becomes apparent even in the averaged crystal structure.

The obtained unit cell volumes of phase IV up to 14 GPa were fitted by 3BM-EOS (Fig. 4c), yielding $K_0 = 18.7(4)$ GPa, $K_0' = 6.8(3)$, and $V_0 = 57.97(4)$ Å³. The unit cell volume extrapolated to 15.1 GPa using these parameters is 42.9 Å³, while the observed unit cell volume of phase V divided by two for comparison is 42.09 Å³ (Table 1), so the volume difference between phase IV and V is 0.8 Å³. Since both phases IV and V are orientationally ordered states, there would be no configurational entropy and probably a small vibrational entropy difference between them owing to the volume difference. Considering the Clausius-Clapeyron slope $dT/dP = \Delta V/\Delta S$, the inclination of the phase boundary between phase IV and V would be positive as shown in Figure 1. More detailed phase relation between phase IV and V would leave open questions here, since we have not investigated low- or high-temperature experiments under such high-pressure conditions, and also noteworthy that the back transition from phase V to IV should be investigated for determining the accurate phase transition boundaries.

Conclusions

We investigated the compression behavior of NH_4Cl using x-ray diffraction under high-pressure and low-temperature conditions. A discontinuity in the unit cell volume was observed at approximately 0.7–1.0 GPa, indicating a first-order phase transition from phase II to phase IV. Low-temperature x-ray diffraction measurements further revealed a slight hysteresis in the phase II–IV transition at ambient pressure, suggesting differences in NH_4^+ ion ordering between cooling and heating processes. Additionally, the structural analysis of phase V demonstrated that N-H...Cl hydrogen bonding contributes to the anisotropic distortion of N-Cl distances. These findings provide new insights into the phase transitions and hydrogen bonding behavior of NH_4Cl under extreme conditions.

Author contributions

KK conceived and designed the research. KK, TM and HK performed x-ray diffraction experiments at BL-18C, PF. SN performed the helium gas loading with assistance from KK and TM. KK and TM analyzed the data and drafted the manuscript. All authors discussed the results and contributed to manuscript preparation.

Conflicts of interest

There are no conflicts to declare.

Data availability

All data shown in this study are available from the corresponding author upon reasonable request.

Acknowledgements

We are grateful to Hiroki Kobayashi and Hayate Ito (The University of Tokyo) for their assistance to the x-ray diffraction experiments. This study was supported by JSPS KAKENHI (Grant Numbers: 21K18154, 18H01936). Crystal structure models in Figs. 1 and 4 are drawn with the VESTA program²⁵.

Notes

- ‡ However, if future research establishes that phases III and V are structurally and thermodynamically identical, it may be more appropriate to unify their nomenclature.
- § We initially tested the compression without any PTMs, however, abnormal recrystallization occurred and coarse crystals were grown, which hampered the precise structure analysis by powder diffraction. The abnormal recrystallization could be caused by heterogeneous stress concentrated around the grain boundary.

References

- (1) Simon, F. Untersuchungen über die spezifische Wärme bei tiefen Temperaturen. *Annalen der Physik* **1922**, 373 (11), 241-280. DOI: <https://doi.org/10.1002/andp.19223731103>.
- (2) Herstein, F. On the mechanism of some first-order enantiotropic solid-state phase transitions: from Simon through Ubbelohde to Mnyukh. *Acta Crystallographica Section B* **2006**, 62 (3), 341-383. DOI: doi:10.1107/S0108768106008640.
- (3) Bridgman, P. W. The P-V-T Relations of NH_4Cl and NH_4Br , and in Particular the Effect of Pressure on the Volume Anomalies. *Phys. Rev.* **1931**, 38 (1), 182-191. DOI: 10.1103/PhysRev.38.182.
- (4) Ren, Q.; Qi, J.; Yu, D.; Zhang, Z.; Song, R.; Song, W.; Yuan, B.; Wang, T.; Ren, W.; Zhang, Z.; Tong, X.; Li, B. Ultrasensitive barocaloric material for room-temperature solid-state refrigeration. *Nat. Commun.* **2022**, 13 (1), 2293. DOI: 10.1038/s41467-022-29997-9.
- (5) Lu, M.; Tian, F.; Zhou, Q.; Cui, T. First principle studies of ammonium chloride under high pressure. *RSC Advances* **2021**, 11 (9), 5149-5155, 10.1039/D0RA09718G. DOI: 10.1039/D0RA09718G.
- (6) Conway, L. J.; Brown, K.; Loveday, J. S.; Hermann, A. Ammonium fluoride's analogy to ice: Possibilities and limitations. *J. Chem. Phys.* **2021**, 154 (20), 204501. DOI: 10.1063/5.0048516.
- (7) Shephard, J. J.; Ling, S.; Sosso, G. C.; Michaelides, A.; Slater, B.; Salzmann, C. G. Is High-Density Amorphous Ice Simply a "Derailed" State along the Ice I to Ice IV Pathway? *J. Phys. Chem. Lett.* **2017**, 8 (7), 1645-1650. DOI: 10.1021/acs.jpclett.7b00492.
- (8) Pistorius, C. W. F. T. Melting Curves and Phase Transitions of the Ammonium Halides to 40 kbar. *J. Chem. Phys.* **1969**, 50 (3), 1436-1442. DOI: 10.1063/1.1671208.
- (9) Ross, R. G.; Sandberg, O. Thermal conductivity and heat capacity of solid phases of NH_4Cl under pressure. *Journal of Physics C: Solid State Physics* **1979**, 12 (18), 3649-3660. DOI: 10.1088/0022-3719/12/18/009.
- (10) Balagurov, A. M.; Kozlenko, D. P.; Savenko, B. N.; Glazkov, V. P.; Somenkov, V. A.; Hull, S. Neutron diffraction study of structural changes in ammonium halides under high pressure. *Physica B: Condensed Matter* **1999**, 265 (1), 92-96. DOI: [https://doi.org/10.1016/S0921-4526\(98\)01331-3](https://doi.org/10.1016/S0921-4526(98)01331-3).
- (11) Heyns, A. M. The effect of pressure on the Raman spectrum of NH_4Cl . *J. Phys. Chem. Solids* **1980**, 41 (7), 769-776. DOI: [https://doi.org/10.1016/0022-3697\(80\)90086-4](https://doi.org/10.1016/0022-3697(80)90086-4).
- (12) Jeon, S.-J.; Porter, R. F.; Ruoff, A. L. High-pressure Raman study of ammonium halides. *Journal of Raman Spectroscopy* **1988**, 19 (3), 179-182. DOI: <https://doi.org/10.1002/jrs.1250190307>.
- (13) Huang, Y.; Huang, X.; Wang, L.; Wu, G.; Duan, D.; Bao, K.; Zhou, Q.; Liu, B.; Cui, T. Structural properties of ammonium iodide under high pressure. *RSC Advances* **2015**, 5 (50), 40336-40340, 10.1039/C5RA04211A. DOI: 10.1039/C5RA04211A.
- (14) Weiner, B. B.; Garland, C. W. Order - Disorder Phenomena. VII. Critical Variations in the Length of NH_4Cl Single Crystals at High Pressures. *J. Chem. Phys.* **1972**, 56 (1), 155-165. DOI: 10.1063/1.1676842.
- (15) Yurtseven, H.; Salihoğlu, S.; Şen, S. λ -transition of NH_4Cl and ND_4Cl at high pressures. *physica status solidi (b)* **2007**, 244 (7), 2589-2596. DOI: <https://doi.org/10.1002/pssb.200642154>.
- (16) Staško, D.; Prchal, J.; Klicpera, M.; Aoki, S.; Murata, K. Pressure media for high pressure experiments, Daphne Oil 7000 series. *High. Press. Res.* **2020**, 40 (4), 525-536. DOI: 10.1080/08957959.2020.1825706.
- (17) Seto, Y.; Nishio-Hamane, D.; Nagai, T.; Sata, N. Development of a Software Suite on X-ray Diffraction Experiments. *The Review of High Pressure Science and Technology* **2010**, 20 (3), 269-276.

- (18) Matsui, M.; Higo, Y.; Okamoto, Y.; Irifune, T.; Funakoshi, K.-I. Simultaneous sound velocity and density measurements of NaCl at high temperatures and pressures: Application as a primary pressure standard. *Am. Mineral.* **2012**, *97* (10), 1670-1675. DOI: 10.2138/am.2012.4136.
- (19) Toby, B. EXPGUI, a graphical user interface for GSAS. *J. Appl. Crystallogr.* **2001**, *34* (2), 210-213. DOI: doi:10.1107/S0021889801002242. Larson, A.; Von Dreele, R. General Structure Analysis System (GSAS). *Los Alamos National Laboratory, Report LAUR-86-748* **2004**.
- (20) Takemura, K.; Sahu, P. Ch.; Kunii, Y.; Toma, Y. Versatile gas-loading system for diamond-anvil cells. *Rev. Sci. Instrum.* **2001**, *72* (10), 3873-3876. DOI: 10.1063/1.1396667.
- (21) Oishi, R.; Yonemura, M.; Nishimaki, Y.; Torii, S.; Hoshikawa, A.; Ishigaki, T.; Morishima, T.; Mori, K.; Kamiyama, T. Rietveld analysis software for J-PARC. *Nuclear Instruments and Methods in Physics Research Section A: Accelerators, Spectrometers, Detectors and Associated Equipment* **2009**, *600* (1), 94-96. DOI: <https://doi.org/10.1016/j.nima.2008.11.056>.
- (22) Dinichert, P. The transformation of ammonium chloride observed by the diffraction of x-rays. *Helvetica Physica Acta* **1942**, *15*, 462-475. Hovi, V.; Mutikainen, P.; Pirinen, J. X-ray investigation of the thermal expansion of NH₄Cl below and above the λ -transition. *Ann. Acad. Sci. Fenn. Ser. A6* **1973**, *464*, 3-12.
- (23) Fortes, A. Accurate and precise lattice parameters of H₂O and D₂O ice Ih between 1.6 and 270 K from high-resolution time-of-flight neutron powder diffraction data. *Acta Crystallographica Section B* **2018**, *74* (2), 196-216. DOI: doi:10.1107/S2052520618002159.
- (24) Funnell, N. P.; Bull, C. L.; Hull, S.; Ridley, C. J. Phase behaviour of ammonium bromide-d₄ under high pressure and low temperature; an average and local structure study. *J. Phys.: Condens. Matter* **2022**, *34* (32), 325401. DOI: 10.1088/1361-648x/ac730b.
- (25) Momma, K.; Izumi, F. VESTA 3 for three-dimensional visualization of crystal, volumetric and morphology data. *J. Appl. Crystallogr.* **2011**, *44* (6), 1272-1276. DOI: doi:10.1107/S0021889811038970.